Metabolically Efficient Codes in The Retina

Vijay Balasubramanian^{1*} and Michael J Berry II^{2*},

¹David Rittenhouse Laboratories, University of Pennsylvania Philadelphia, PA 19104, U.S.A. Email: vijay@endive.hep.upenn.edu

²Department of Molecular Biology, Princeton University, Princeton, NJ 08544, U.S.A. Email: berry@princeton.edu

April 26, 2001

Abstract

We tested the hypothesis that the neural code of retinal ganglion cells is optimized to transmit visual information at minimal metabolic cost. Under a broad ensemble of light patterns, ganglion cell spike trains consisted of sparse, precise bursts of spikes. These bursts were viewed as independent neural symbols. The noise in each burst was measured via repeated presentation of the visual stimulus, and the energy cost was estimated from the total charge flow in a biophysically realistic model of ganglion cell spiking. Given these costs and noise, the theory of efficient codes predicts an optimal distribution of symbol usage. Symbols that are either noisy or metabolically costly are suppressed in this optimal code. We found excellent qualitative and quantitative agreement with the measured distribution of burst sizes for ganglion cells in the tiger salamander retina.

^{*}Both authors contributed equally to this work.

Introduction

Optimization principles remain a fundamental approach to understanding the structure and function of the nervous system. By quantifying the performance of neurons, information theory provides very general tools for constructing such principles. An intuitive design, especially for the sensory periphery, is that a neuron should maximize the mutual information between input and output, subject to realistic constraints. Noise, either in the input or added by the neuron, is a fundamental constraint. Several researchers ([Barlow, 1961]; [Atick, 1992]; [van Hateren, 1992]) have had success predicting how the receptive fields of retinal neurons should be organized to maximize the transmission of information about natural visual images. This success might lead one to imagine that many neurons strive to maximize information transmission.

However, there is a serious difficulty: spiking neurons, which constitute the vast majority of neurons in the vertebrate brain, produce action potentials at average rates far below the rate that maximizes transmitted information. A simple estimate can be made as follows. Since the maximum firing rate is set by the refractory period $\mu \sim 5$ ms, an axon would achieve its highest entropy by firing at a rate that gives a 1/2probability of spiking in each possible time bin, $r^* = 1/(2\mu) \sim 100$ Hz. Timing jitter can be expected to increase the effective bin size for spiking beyond μ and hence lower the firing rate that achieves maximum information transmission. However, measurements from a number of neurons under realistic stimulation show timing precision of < 5 ms ([Berry et.al., 1997]; [de Ruyter et.al., 1997]; [Buracas et.al., 1998]). Thus, one expects that most neurons would achieve maximal information transmission at a firing rate close to $r^* \sim 100$ Hz. Instead, many neurons fire much less frequently: for instance, ganglion cells in the salamander retina fire 1 to 5 spikes/sec under varied stimulation [Berry et.al., 1997], and pyramidal neurons in the rat cortex fire at 1 to 4 spikes/sec ([Schoenbaum, et.al., 1999]; [Fanselow and Nicolelis, 1999]), to name just a few. Therefore, one must conclude either that these neurons are not well designed for information transmission or that other considerations are important.

In fact, neurons are some of the most energy intensive cells in the body [Wong-Riley, 1989], and spikes comprise a significant portion of their energy usage ([Siesjo, 1978]; [Ames, 2000]; [McIlwain and Bachelard, 1985]; [Atwell and Laughlin, 2001]). This suggests that neural codes might be constrained by a requirement of energy efficiency. Previous work has developed a general theory of energy-efficient codes that predicts the optimal usage distribution of a set of discrete, independent neural symbols, each subject to an energy cost and corrupted by noise ([Levy and Baxter, 1996]; [Balasubramanian et.al., 2001]; [de Polavieja, 2001]). We used this prediction to make a quantitative test of the hypothesis that the neural code of retinal ganglion cells is energy efficient. Under a wide variety of stimulus conditions, the output of ganglion cells is a sparse set of discrete firing events [Berry et.al., 1997]. Each firing event is a

tight burst that we view as a composite neural symbol characterized by its number of spikes. The noise of each firing event was measured by repeated presentations of the same stimulus, and the energy cost was estimated by simulations of the ionic current flow during spiking. The theoretically optimal distribution of burst sizes was found to be in both qualitative and quantitative agreement with experiment.

MATERIALS AND METHODS

Experimental Methods

Experiments were performed on isolated retinas from the larval tiger salamander (Ambystoma tigrinum tigrinum). The retina was perfused with Ringer's medium (110 mM NaCl, 22 mM NaHCO₃, 2.5 mM KCl, 1.6 mM MgCl₂, 1 mM CaCl₂, 10 mM D-glucose), which was oxygenated by continuously bubbling a 95%/5% O₂/CO₂ mixture through it. Action potentials from retinal ganglion cells were recorded using a multi-electrode array (see [Berry et.al., 1997] and [Meister et al., 1994] for further details) while the preparation was at room temperature. This temperature is realistic for tiger salamanders in their natural habitat [Roth, 1987]. The retina was stimulated with illumination from a computer monitor that was focussed onto the photoreceptor layer. Stimuli were drawn from an ensemble of spatially uniform random flicker, in which intensity values for the entire screen were chosen every 30 ms from a Gaussian distribution. The mean light level was in the phototopic range for salamander (7 mW/m^2) , and the temporal root-mean-squared fluctuation (contrast) was 35% of the mean. This level of contrast approximates that found under more natural viewing conditions [van der Schaaf and van Hateren, 1996]. Similar experiments were performed using spatially modulated stimuli, in which square regions of the computer monitor flickered independently, yielding ganglion cell responses similar to the present study (data not shown).

Spike trains were recorded during 30 or 60 repeated presentations of stimulus sequences lasting from 120 s to 540 s. Total recording times ranged from 120 min up to 270 min, with an average of 222 min. Multiple tests of stationarity were employed to screen for ganglion cells whose function remained constant during the experiment. The overall response, quantified by the average firing rate, remained stable to better than 5% (average stability over all ganglion cells, 3.6%). The noisiness of the response, quantified by the timing precision and number precision (see [Berry et.al., 1997] for details), remained constant to better than 10% (averages 9.1% and 8.2%, respectively). A total of 12 ganglion cells passed these tests of stationarity over long enough recording times to be useful to our analysis. They were all fast OFF-type cells, identified by their unique reverse correlation to random flicker stimulation [Smirnakis et al., 1997]. These cells resemble Y cells in the cat and M cells in the monkey. In the tiger salamander, as in most amphibians, the overwhelming majority (80% - 90%) of ganglion cells are OFF-type ([Smirnakis et al., 1997]; [Roth, 1987]).

Firing Event Identification

Under random flicker stimulation, salamander ganglion cells respond in sparse, highly precise firing "events" [Berry et.al., 1997]. Most events were easily identified as single peaks in the firing rate flanked by periods of silence. But in some instances, more ambiguous peaks in the firing rate were observed. In order to provide a consistent definition of firing events, we identified event boundaries as reproducible minima in the firing rate. For each minimum ν , the ratio of the firing rate at its adjacent peaks (p_1, p_2) to that at the minimum was required to exceed a threshold value, $\sqrt{p_1 p_2}/\nu \phi$, with 95% confidence. The threshold was set to $\phi = 2$; event boundaries were rather insensitive to its value (see [Berry et.al., 1997] for addition details). Once event boundaries were drawn, all spikes between succesive boundaries were assigned to a single event. We denote the number of spikes at event number a on stimulus trial b as n_{ab} . If no spikes were observed in a given trial, n_{ab} was zero. The average number of spikes in that event is $N_a = \langle n_{ab} \rangle_b$, and the variance is $\text{var}(N_a) = \langle n^2 \rangle - \langle n \rangle^2$.

Energy Efficient Neural Codes

The properties of an optimally energy efficient neural code were defined in earlier work ([Levy and Baxter, 1996]; [Balasubramanian et.al., 2001]; [de Polavieja, 2001]). Here, we imagine that a neural circuit maps stimuli deterministically onto a discrete set of desired neural symbols $\{Y\}$, and that noise is added before the output of actual neural symbols $\{Z\}$ (see Fig. 2A). The goal of an energy efficient code is to find the probability p_k of using each output symbol z_k that optimizes information transmission per unit metabolic cost. In the absence of noise, the solution is:

$$p_k = e^{-\beta E_k} \tag{1}$$

where β is set such that $\sum_k e^{-\beta E_k} = 1$. However, noise profoundly alters the optimal symbol distribution [Balasubramanian et.al., 2001] and should therefore be carefully measured in a biological system and included in the theory.

Noise is expressed as a transition matrix $Q_{k|j}$ that describes the likelihood that the intended message or presymbol y_j emerges from the channel as z_k . Given this "noise matrix", an iterative algorithm generalizing classic work by Arimoto and Blahut ([Arimoto, 1972]; [Blahut, 1972]; [Blahut, 1987]) computes the symbol distribution that optimizes information transmission at a fixed average cost E. This algorithm is summarized as follows:

- 1. Choose arbitrary nonzero probabilities for the presymbols $q_i^{(0)}$
- 2. For iteration $t = 0, 1, 2, \dots$ repeat:
 - (a) Find the probability that observed output symbol z_k arose from the presymbol y_j : $\hat{P}_{j|k}^{(t)} \leftarrow \frac{q_j^{(t)}Q_{k|j}}{\sum_i q_j^{(t)}Q_{k|j}}$

(b) Update the optimal distribution of presymbols according to

$$q_j^{(t+1)} \leftarrow \frac{e^{-\beta^{(t+1)}E_j - \hat{H}_j^{(t)}}}{\sum e^{-\beta^{(t+1)}E_j - \hat{H}_j^{(t)}}}$$
(2)

with $\beta^{(t+1)}$ chosen numerically so that $\sum_j q_j^{(t+1)} E_j = E$. Here we defined $\hat{H}_j^{(t)} \equiv -\sum_k Q_{k|j} \log \hat{P}_{j|k}^{(t)}$.

(c) If
$$q_j^{(t+1)}$$
 close to $q_j^{(t)}$ stop.

We call the final, optimal probabilities of presymbols q_j and define $\hat{P}_{j|k}$ and \hat{H}_j in terms of q_j . The optimal probability of output symbol z_k is then given by $p_k = \sum_j Q_{k|j} q_j$.

Using this algorithm, we can always find the probability distribution of coding symbols that optimizes the mutual information they transmit about a sensory stimulus at a fixed average cost E. In bits, this maximized mutual information is given by $I = -\sum_j q_j (\ln q_j + \hat{H}_j)$, while the average energy used per symbol transmitted is $E = \sum_j q_j E_j$. Numerical optimization of I/E then yields the code that maximizes information transmission per unit metabolic cost. The necessary ingredients of this model are the energy cost of each output symbol, E_k , and the noise in each presymbol, $Q_{k|j}$.

The energy efficient codes derived in this manner have three salient features that are relevant for this study. First, more energetic symbols are suppressed in the optimal distribution. Second, noisier symbols are also suppressed. Both these facts are illustrated in panels B and C of Fig. 2. Finally, a surprising property of metabolically efficient codes is that the distribution over symbols that maximizes bits per energy is actually invariant under rescalings of the energy costs $E_n \to \lambda E_n$ where λ is some fixed number (see [Balasubramanian et.al., 2001] for a proof). This fact allows us to eliminate one parameter in our model; the linear energy model $E_n = a_1 + a_2 n$ can be rescaled by a factor of $1/a_1$ to $E_n = 1 + b n$, while leaving the optimal distribution invariant. We interpret the resulting parameter $b = a_2/a_1$ as the relative cost of a spike compared to the baseline cost of keeping the cell alive.

Classifying Presymbols

In order to provide a consistent and statistically significant classification of firing events into presymbols, we used the following algorithm:

- (1) Compare the number of observations of the most common burst size B_1 to the number of observations of the next most common B_2 . If B_1 exceeds B_2 with 95% confidence (assuming Poisson counting statistics), then the event arises from an integer presymbol corresponding to the most common burst size. Most events (68%) were classified as arising from integer presymbols.
- (2) If B_1 does not exceed B_2 , compare B_1 to the observations of the third most common burst size B_3 . If B_1 exceeds B_3 with 95% confidence, then the event is a

half-integer presymbol corresponding to the two most common burst sizes. The vast majority of these events were split between successive spike counts, such as 1 and 2 spike bursts, accounting for 28% of all events. The remaining 0.2% of all events had bimodal burst size distributions, often between 0 and 2 spikes. Because the latter events were so rare, we simply treated them as integer presymbols corresponding to the most common burst size.

- (3) If B_1 does not exceed B_3 , check whether the three most common burst sizes have successive values. If so, check if the most common burst size is flanked by the next two most common. In this case, assume that the event is a noisier integer event corresponding to the most common burst size (2% of all events fell in this category). Otherwise, assume that this is a noisier half-integer event characterized by the two most common burst sizes (2% of all events fell in this category).
- (4) If the three most common burst sizes were not successive, we could not clearly characterize the presymbol. As only 0.05% of all events were in this final category, we again assumed that they were noisy integer events corresponding to their most common burst size.

The Results section motivates the classification algorithm above in terms of the measured characteristics of burst size distributions for different events.

Burst Size Distributions and Noise Matrices

For each ganglion cell, we compiled a burst size distribution P(z) from the spike counts for individual events and trials, n_{ab} . Increasingly large bursts were increasingly rare, and their probability consequently had large uncertainty due to random error. Therefore, in our analysis we only included bursts up to a maximum burst size z_{max} . We denote the number of observations of burst size z in a single stimulus trial by N(z). The probability that a randomly selected burst in the trial has size z then is $P(z) = N(z)/\sum_z N(z)$, where we only include z up to z_{max} . Our criterion for choosing z_{max} was that $\sim 98\%$ of all bursts were included. Over our population of ganglion cells, z_{max} ranged from 4 up to 6 spikes with an average of 4.6, and the fraction of all bursts thus included ranged from 96.8% to 99.6% with an average of 98.7%.

We compiled the noise matrix $Q_{z|y}$ by estimating which presymbol y_a gave rise to each firing event (see Classifying Presymbols) and adding the histogram of n_{ab} for event a over repeated trials b to the row of Q corresponding to y_a . We denote the number of observations of burst size z given presymbol y as $L_{z|y}$, and the number of observations of presymbol y as M_y . Each row of the noise matrix was separately normalized by the number of observed presymbols, $Q_{z|y} = L_{z|y}/(M_y R)$, where R is the number of stimulus repeats. This normalization gives $\sum_z Q_{z|y} = 1$ as it should in order that $Q_{z|y}$ describe the probability that a given presymbol y produces the output z. As discussed above, the measured burst size distribution was truncated at a given z_{max} for each cell, which can create unwanted "edge effects" in the theoretical

analysis of the energy optimal burst size distribution. In order to avoid these edge effects, we kept burst sizes greater than z_{max} in the noise matrix. However, after the theoretical prediction of the optimal burst size distribution $P^*(z)$ was obtained, we truncated it at $z = z_{\text{max}}$ and re-normalized to unity, $\sum_{z=1}^{z_{\text{max}}} P^*(z) = 1$. This allowed us to compare the predictions of the theory properly with the measured distribution P(z).

Error Analysis

For making quantitative comparisons between optimal and actual neural codes, we must treat the uncertainty in our measurements properly. Assigning error bars to the burst size distribution is not trivial, because repeated presentations of the stimulus do not yield independent measurements of the burst size distribution: these measurements are related to each other by the noise matrix. However, we can use the fact that random flicker is completely uncorrelated from one stimulus frame to the next. Therefore, the stimulus patterns that cause each type of firing event occur independently and with a constant probability per unit time. The number of presymbols of each type elicited by a stimulus sequence of fixed length will vary with Poisson statistics:

$$Var[M_y] = M_y. (3)$$

For each presymbol, variations in the number of output spikes observed on different stimulus trials are also independent and obey Poisson statistics. This implies that variations in $L_{z|y}$, the number of observations of z given presymbol y, are also Poisson:

$$Var[L_{z|y}] = L_{z|y}. (4)$$

We can use eqs. (3) and (4) to find the error Var(N(z)). By definition of the noise matrix, $N(z) = \sum_{y} Q_{z|y} M_y = (1/R) \sum_{y} L_{z|y}$. Therefore:

$$Var[N(z)] = (1/R) \sum_{y} Var(L_{z|y}) = (1/R) \sum_{y} L_{z|y} = N(z).$$
 (5)

In order to find the error in the probability distribution over burst sizes P(z), we use standard error propagation:

$$P(z) = \frac{N(z)}{\sum_{z'} N(z')} \tag{6}$$

$$Var[P(z)] = \left(\frac{1}{\sum_{z'} N(z')} + \frac{N(z)}{(\sum_{z'} N(z'))^2}\right) Var[N(z)]$$

$$= \left(\frac{\sum_{z'} N(z') + N(z)}{(\sum_{z'} N(z'))^2}\right) N(z)$$
(7)

As we have discussed, a crucial input to the theory is the experimentally measured noise in each ganglion cell. Poisson variation in the number of presymbols y and

the resulting observations of outputs z imply that the entries in the noise matrix $Q_{z|y} = L_{z|y}/M_yR$ have variances

$$Var[Q_{z|y}] = \frac{2L_{z|y}}{M_y R} = 2Q_{z|y}$$
 (8)

where we have once again used standard error propagation. Since we use a numerical algorithm to derive the metabolically optimal code, it is not possible to derive an analytic expression for the error bars in the theoretical prediction. Furthermore, doing a complete numerical error propagation is prohibitively time consuming. Instead, we have estimated the effects of the measurement errors on the theory by propagating the most important uncertainties, namely those in the diagonal entries of the noise matrix, through the algorithm that determines the optimal metabolically efficient code. The resulting errors are reported in Fig. 7 by including the maximum and minimum deviations in the predicted probability for each symbol when the diagonal entries of the noise matrix were perturbed by plus or minus one standard deviation. In the limit of small errors, this min-max error is similar to the result of standard error propagation. Further discussion appears in the Results sections below.

Ion Channel Simulations

We studied the energy cost associated with electrical activity using a single compartment model of tiger salamander ganglion cells due to Fohlmeister and Miller (FM) [Fohlmeister and Miller, 1997]. This model included five membrane currents: voltage gated sodium (I_{Na}) , voltage gated calcium (I_{Ca}) , delayed rectifier potassium (I_{K}) , inactivating potassium (I_{A}) , and calcium-gated potassium current $(I_{\text{K,Ca}})$. In addition to these ionic currents the model includes an effective leak and a capacitance leading to the equivalent circuit equation:

$$I_{\text{stim}} = C_m \frac{dV}{dt} + \bar{g}_{\text{Na}} m^3 h (V - V_{\text{Na}}) + \bar{g}_{\text{Ca}} c^3 (V - V_{\text{Ca}}) + (\bar{g}_{\text{K}} n^4 + \bar{g}_{\text{A}} a^3 h_{\text{A}} + g_{\text{K,Ca}}) (V - V_{\text{K}}) + \bar{g}_{\text{leak}} (V - V_{\text{leak}})$$
(9)

This equation holds for every patch of cell membrane; so we specify conductances in units of mS/cm² and therefore describe the current density through the ganglion cell membrane. The cell capacitance (C_m) , the Na⁺ and K⁺ reversal potentials $(V_{\text{Na}}, V_{\text{K}})$ and the conductances \bar{g}_{Na} , \bar{g}_{Ca} , \bar{g}_{K} , \bar{g}_{A} were all given by constants specified in Table 1 of [Fohlmeister and Miller, 1997]. The leak reversal potential was chosen as $V_{\text{leak}} = -65 \,\text{mV}$, so that after a long period with $I_{\text{stim}} = 0$, the membrane approaches a resting potential of $V = V_{\text{leak}}$. The leak conductance was chosen to be $\bar{g}_{\text{leak}} = 0.05 \,\text{mS/cm}^2$. (This is the value given in the text of [Fohlmeister and Miller, 1997] and not in their Table 1.) The calcium reversal potential was modelled dynamically by the Nernst equation:

$$V_{\text{Ca}} = \frac{RT}{2F} \ln \left[\frac{[\text{Ca}^{2+}]_e}{[\text{Ca}^{2+}]_i(t)} \right]$$

$$\tag{10}$$

$$\frac{d[Ca^{2+}]_i}{dt} = -\frac{3I_{Ca}}{2Fr} - \frac{([Ca^{2+}]_i - [Ca^{2+}]_{res})}{\tau_{Ca}}$$
(11)

Here R is the gas constant, T is temperature, F is the Faraday constant, r is the radius of the cell, $[\mathrm{Ca^{2+}}]_e$, $[\mathrm{Ca^{2+}}]_i$, and $[\mathrm{Ca^{2+}}]_{\mathrm{res}}$ are the external, intercellular, and residual intracellular calcium concentrations respectively. τ_{Ca} is the time constant for the removal of calcium from the intracellular space either by pumping out of the cell or be sequestering in internal stores. These parameters were extracted from the text of [Fohlmeister and Miller, 1997] and are specified in the table below. The conductance of the calcium gated potassium channel varies with calcium concentration as:

$$g_{K,Ca} = \bar{g}_{K,Ca} \frac{([Ca^{2+}]_i/[Ca^{2+}]_{diss})^2}{1 + ([Ca^{2+}]_i/[Ca^{2+}]_{diss})^2}$$
(12)

where $[Ca^{2+}]_{diss}$ is the calcium dissociation constant for the calcium gated potassium channel. Finally, the state variables of the voltage gated channels obey Hodgkin-Huxley equations:

$$\frac{dx}{dt} = -(\alpha_x + \beta_x) x + \alpha_x \tag{13}$$

where x is any one of (m, h, c, n, h_A) . The parameters α_x and β_x are themselves dependent on the membrane potential V as described in Fohlmeister and Miller. (Note that the parameter E in Fig. 1 of [Fohlmeister and Miller, 1997] should be understood as the membrane potential V.) In summary, we used the following parameters in our simulations:

$\bar{g}_{\mathrm{Na}} = 50 \mathrm{mS/cm^2}$	$\bar{g}_{\mathrm{Ca}} = 2.2 \mathrm{mS/cm^2}$	$\bar{g}_{\mathrm{K}} = 12 \mathrm{mS/cm^2}$	$\bar{g}_{\mathrm{A}} = 36 \mathrm{mS/cm^2}$
$\bar{g}_{\mathrm{K,Ca}} = 0.05 \mathrm{mS/cm^2}$	$\bar{g}_{\mathrm{leak}} = 0.05 \mathrm{mS/cm^2}$	$V_{\rm Na} = 35 mV$	$V_{\rm K} = -75 mV$
$V_{\text{leak}} = -65 mV$	$C_m = 1 \mu\text{F/cm}^2$	$T = 22 ^{\circ}C$	r = 0.0025 cm
RT/F = 25.43 mV	Fr = 241.22 cm	$\tau_{\mathrm{Ca}} = 50 ms$	$[\mathrm{Ca}^{2+}]_{\mathrm{diss}} = 1\mu M$
$[\text{Ca}^{2+}]_{\text{res}} = 0.1 \mu M$	$[\mathrm{Ca}^{2+}]_{\mathrm{e}} = 1800 \mu M$		

With these parameters fixed, we studied the energetics of spiking by stimulating the model with brief current pulses following long resting periods. The charge flow in each ionic channel was obtained by integrating the corresponding current as a function of time. The ATP consumption in ganglion cell soma required for transporting this charge will be linear in the amount of charge, allowing us to determine how the energy cost depends on the number of spikes and time intervals between spikes in a burst. The results of these simulations are described in Results.

RESULTS

Burst size distributions

Recordings were made from ganglion cells in the larval tiger salamander retina while stimulated with the diverse temporal patterns of light found in spatially uniform flicker (see Materials and Methods). This paper describes results from 12 ganglion cells of the fast OFF type. Under random flicker stimulation, these ganglion cells respond in sparse, highly precise episodes of firing ([Berry et.al., 1997]; [Berry and Meister, 1998]; [Meister and Berry, 1999]). These firing "events" were tight bursts containing one to eight spikes with inter-spike intervals of 5 to 10 ms. Their first spike was elicited with timing that typically jittered by ~ 4 ms from one repeated stimulus presentation to the next. The total number of spikes in an event typically varied by ~ 0.5 spike. In between events, the spontaneous firing rate was strictly zero. Events occurred at rates of 1 to 3 per second, with inter-event time intervals broadly distributed from 50 ms up to 3 s. Because of their high precision, each firing event can serve as an individual visual message of high fidelity. Because of the long inter-event time intervals and the consequently weak correlations between successive firing events, each event can serve as an independent visual message. This led us to consider each firing event as a composite coding symbol, characterized by its time of occurrence and total number of spikes.

Because events with different numbers of spikes can encode different visual messages, this paper focuses on the distribution of burst sizes chosen by retinal ganglion cells to represent a broad ensemble of stimuli. Fig. 1 shows such distributions for four cells along with error bars that reflect the expected Poisson variation for stimuli drawn from the same ensemble (see Materials and Methods). A characteristic feature shared by all cells is the sharp falloff of bursts of large size. An energy efficient code would behave in this way since large bursts are expected to cost more energy. Some of the cells have the surprising feature of sharp suppression of small bursts (Fig. 1B), and most show a flattening at small bursts (Figs. 1C and 1D). Naively, this seems to point away from energy efficiency as an organizing principle for the retinal code since smaller bursts cost less energy. However, efficient coding also requires the suppression of noisy symbols, and as we shall see, small bursts are suppressed in precisely those cells where these bursts are not reliably produced from trial to trial.

Structure of the model

In order to assess the energy efficiency of the retinal code, we developed a simple model of a sensory system in which the properties of an optimally energy efficient code could be solved [Balasubramanian et.al., 2001]. In this model, the action of a neural circuit was idealized as occurring in three stages: stimuli in the external world $\{S\}$ are detected by an array of sensors and converted into neural signals $\{X\}$, these signals are encoded deterministically into a discrete set of composite symbols $\{Y\}$, and finally noise is added before the output $\{Z\}$ emerges (see Fig. 2A). For the retina, S would be patterns of light projected by the optics of the eye, X would be the response of the array of photoreceptors, and Z would be the spike train produced by one or more retinal ganglion cell. The intermediate variable Y is not directly observable; we refer to its possible values $\{y_0, y_1, \dots, y_n\}$ as presymbols.

In the model, the output $\{Z\}$ is a string of discrete, independent neural symbols

 $\{z_0, z_1, \dots, z_n\}$. Each symbol z_k has an energy cost E_k associated with its production. In the case of the retina, individual firing events are viewed as the output symbols. Firing events are distinguished only by their number of spikes: z_1 is a 1-spike burst, z_2 is a 2-spike burst, etc. We add a symbol z_0 representing every 50 ms period of silence. (Our results display very little sensitivity to the value of the time bin used to discretize periods of silence, as we have checked by picking a variety of time bins.) Because spiking represents a significant energy expenditure for a neuron, firing events with different numbers of spikes have significantly different energy costs. We will argue below that the energy cost of a burst is linearly related to its number of spikes.

Given a set of costs $\{E_0, E_1, \dots, E_n\}$ for the output symbols z_k , and a noise matrix $Q_{k|j} = \Pr(z_k|y_j)$ which gives the probability that a presymbol y_j yields an output symbol z_k , we can calculate the distribution of symbols z_k which optimizes the information transmitted per unit metabolic cost (see Methods) [Balasubramanian et.al., 2001]. The theory predicts that both noisy and energy expensive symbols are suppressed in the optimal code. For example, Figs. 2B and 2C show a model with 6 input and 6 output symbols with energies $E_k = k$. In the absence of noise, the symbol y_j is transmitted as $z_k = y_j$, and bits per energy is maximized when the usage distribution of outputs z_k is exponential $(p_k = e^{-\beta E_k})$. Fig. 2B shows that the addition of uniform noise distorts the optimal symbol distribution, with a particularly strong effect on the symbol y_1 . Fig. 2C shows that adding noise only to y_3 leads to marked suppression in its use, since this symbol is then not a reliable conveyor of information. Indeed, it is shown in [Balasubramanian et.al., 2001] that small changes in the noise can result in large changes in the optimal distribution of output symbols. So, to study efficient coding by a ganglion cell, we must carefully characterize its noise.

Noise in ganglion cells

Repeated presentations of the same input to the retina lead to a distribution of output burst sizes for each firing event. Fig. 3A plots the variance of the burst size distribution of a given event against its mean. Most values have var(N) < 0.5, indicating that the number of spikes in a firing event is precisely determined by the stimulus. The solid line at the bottom of the graph shows the theoretical lower bound on the variance of events with a given mean, obtained when the event uses only outputs n and n-1 with the appropriate proportions. This theoretical lower bound drops to zero for integer values of the mean spike number and rises to 0.25 for half-integer values. A corresponding pattern is seen for the actual firing events: lower variance occurs near integer values of the mean spike number. This pattern is demonstrated by the thick line in Fig. 3A, which is an average over the observed variance of all events as a function of mean burst size.

This difference between high and low variance events arises fundamentally from the nature of the mapping between the continuous patterns of light occurring in the environment and the discrete outputs of the retina. The set of all patterns of light constitutes a high-dimensional space of stimuli, and we can view the retinal mapping as dividing stimulus space into regions corresponding to presymbols {Y} (see Fig. 3B for a schematic). Noise has the effect of mapping a given stimulus onto a nearby location in stimulus space. When the input starts out near the boundary between two presymbols, noise will be much more likely to change the resulting output symbol than if the stimulus is far from the boundary. For example, Fig. 3B shows regions of stimulus space corresponding to 1-spike and 2-spike outputs. Inputs that lie in the "core" (unshaded) of each region will be mapped more reliably to output burst sizes, while inputs that lie in the "boundary" (shaded) regions will be noisier. As long as the outputs of a neural circuit are discrete, there will exist boundary regions in the input space that are more susceptible to noise.

If the retinal code is designed for efficient transmission of visual information, its input-output map should attempt to reduce noise in the output. Fig. 3C displays the number of events for a typical ganglion cell as a function of mean burst size. Events with an average integer number of spikes are more common than those with a half-integer number. As integer events tend to have lower noise, this bias will have the effect of reducing the overall variability of output symbols. This dominance of "core" events over "boundary" events is not automatic. For example, if the input-output map in Fig. 3B contained a great many small disjoint regions mapping to the same output, then the boundary regions could be greater in size than the cores. Furthermore, a simple model of the spiking process, such as a linear filter followed by a static non-linear function that is monotonic, would not emphasize integer events over half-integer. The fact that the stimulus-response mapping of ganglion cells emphasizes core regions suggests that the retina can be sensitive to minimizing its own noise. It also suggests that we should treat core presymbols distinctly from boundary presymbols when characterizing the cell's noise.

Defining the noise matrix

The noise matrix in the model, $Q_{k|j}$, describes the transition probability between presymbols y_j and observed burst sizes z_k . The presymbols y_j are idealized, noise-free versions of the circuit's desired output z_k . As noise in the retina originates already at the level of photon absorption by the photoreceptors, there is actually no place in the retinal circuit where one can attempt to measure y_j . However, the mapping from $X \to Y$ in Fig. 2 is deterministic, so we can associate a unique value of y_j with each firing event. Because every single observation of a firing event is corrupted by noise, we must observe many instances of every firing event to determine y. Our task is to use the distribution of burst sizes for each firing event to infer that event's presymbol.

As the variability in spike number was very low, most firing events had a narrow, unimodal distribution of burst sizes. Some of these distributions had their peak at a single spike count, while others had a peak shared between two successive burst sizes.

The former case corresponds to a core or integer presymbol, with a value equivalent to the most common burst size (see Fig. 4A). The latter case corresponds to a boundary or half-integer presymbol, split between two successive burst sizes (see Fig. 4B). A small percentage of events had bimodal burst size distributions (see Fig. 4C) or had peaks spread among three or more burst sizes. These events were not well characterized by either integer or half-integer presymbols, but they occurred so infrequently (less than 0.2% of all events) that their awkward classification should not effect our results appreciably. The algorithm used to classify presymbols is described in Materials and Methods. Fig. 4D shows the typical structure of a noise matrix. The block on the jth row and kth column represents the value of $Q_{k|j}$ in the shading depth – darker colours represent larger entries. Notice that integer presymbols are mostly mapped onto single output burst sizes, while half-integer presymbols are mostly mapped onto two burst sizes.

Energetics of spiking

In addition to the noise matrix, the second ingredient we need in order to compare the theory of energy-efficient codes to experimental burst-size distributions is the energy cost of each neural symbol. A significant component of the total energy cost of a neuron results from its electrical signaling ([Siesjo, 1978]; [Laughlin et.al., 1998]; [Atwell and Laughlin, 2001]). In particular, action potentials are accompanied by large ionic currents that must then be reversed by pumps at a cost in energy. For instance, Na^+/K^+ ATP-ase, the most common pump in the nervous sytem, uses one molecule of ATP to pump 3 Na^+ out of the cell and 2 K^+ in to the cell. By estimating the total charge flow during a burst, we can consequently estimate the energy cost of that burst.

We studied a single compartment model of the tiger salamander ganglion cell developed by Fohlmeister and Miller (FM) (see Materials and Methods). Their model used six ionic currents with conductance parameters set to closely match the cell membrane voltage measured during spikes and bursts [Fohlmeister and Miller, 1997]. We excited the FM model with current pulses of increasing duration and amplitude to produce bursts of action potentials. Fig. 5A shows an example of three different current pulses and the resulting bursts of voltage spikes. Fig. 5B shows the ionic current for each channel type. The total charge flow in each of these channel types was computed for a variety of burst sizes by integrating the ionic current. The results are displayed in Fig. 6, along with a linear fit to the data from the delayed-rectified K⁺ current.

Clearly the charge flow, and hence the ATP consumption, is linear with burst size in the FM model and insensitive to the time intervals between spikes in a burst. What is more, the total charge flow associated with action potentials greatly exceeds the resting charge leakage through the cell membrane. These results held for all the amplitudes and durations of injected current that were studied. While there are

certainly other costs and constraints relevant to biological information processing (see the Discussion), this shows that the energy cost of producing bursts in real ganglion cells is likely to be both large and linear in burst size. Therefore, it is reasonable to assume such a linear energy cost model when assessing the energy efficiency of the retinal code.

Theory meets experiment

Accordingly, we assume that a burst of size n has a cost linear in n: $E_n = E_0 + E_s n$. Here, E_0 is interpreted as the cost of 50 ms of silence, and E_s is the added cost of a single spike. Since codes that maximize bits per energy are invariant under rescalings of the cost model: $E_n \to \lambda E_n$ [Balasubramanian et.al., 2001], we can rescale the costs by $1/E_0$ and arrive at

$$E_n = 1 + b n \tag{14}$$

as a one-parameter model of the cost of a burst of size n. The energy slope $b = E_s/E_0$ is the ratio of the cost of producing a spike to the cost of 50 ms of silence. Given the typical ~ 5 ms refractory period between action potentials, a slope of b=1 would imply that an action potential is of order 10 times as expensive as an equal duration of silence.

With the measured noise and the above linear cost, we used the algorithm presented in Materials and Methods to compute the energy-efficient code for different slope parameters b. The number of zero symbols $N(z_0)$ depends on the time bin used to discretize silence. Because our choice of a 50 ms time bin is arbitrary, we left the zero symbol out of the burst size distribution that we attempted to fit with our theory. Furthermore, large bursts were too infrequent to use in our analysis, so we truncated the distribution at a largest burst size z_{max} (see Materials and Methods). Therefore, after computing the optimal distribution over all output symbols in our model $(0,1,2,\cdots)$, we dropped the 0 as well bursts with sizes greater than z_{max} . We then renormalized the theoretical optimal distribution over finite sized bursts $(1,2,\cdots,z_{max})$. This enabled direct comparison with the experimentally measured distribution of burst sizes. For each cell in our data set we performed fits of the theory to the experimentally measured distribution by varying the energy slope b and minimizing χ^2 . Excellent agreement was found between theory and experiment as summarized in Fig. 7.

Qualitative Agreements: Figs. 7 shows representative fits for four cells and display excellent qualitative agreement. For all cells, the sharp falloff of large bursts was accurately reproduced by the theory. Most cells had some suppression of 1-spike bursts. Interestingly, these cells also had higher noise in the 1-spike bursts, which were consequently suppressed in the theoretical efficient code. Some cells showed a marked dip in the use of small bursts (e.g. Fig. 7B). As shown, such dips were also reproduced by the theory, again because of the suppressed use of noisy symbols in an efficient code. It is striking that the decreased use of noisy symbols that would be

predicted by information theory is reproduced in the experimental data.

Quantitative Agreements: Fig. 8A shows the χ^2 per degree of freedom plotted against the energy slope b values obtained from fits to each cell. (χ^2 per degree of freedom is defined as $\chi^2/(N-1)$, where the total χ^2 for the fit is normalized by the number of fit points minus the number of parameters. Whenever we refer to χ^2 in the text it should be understood as χ^2 per degree of freedom.) The open squares show the values obtained by fitting with the empirically measured noise matrix. Low χ^2 values are obtained for all cells. The higher values typically occur when the fit fails to match at one point leading to a large χ^2 contribution. For instance, notice in Fig. 7C that $\chi^2 = 7.2$ due to a large mistmatch in the 5-spike burst, even though the fit of theory to experiment looks quite good to the eye.

Because each element of the experimentally measured noise matrix has error bars, the theoretical burst size distribution also has some uncertainty. This uncertainty is shown as the range bars in Fig. 8A and was computed by propagating the errors in the noise matrix numerically through the theory (see Materials and Methods). The large ranges again occur because some perturbations of the noise matrix led to a bad fit at one point. The ranges in the optimal symbol probabilities produced by perturbing the noise matrix are displayed in Figs. 7 as the thinner upper and lower lines, showing that the fits remain very similar under perturbations in the noise matrix.

The large variation in energy slope b found within a population of ganglion cells of nominally the same functional type may seem surprising. However, this group of cells also had a large range of overall firing rates (roughly a factor of 10), despite the fact that the stimuli were statistically identical for all of them. If ganglion cells are implementing an energy efficient code, one expects that a cell having a small incremental cost of spiking (i.e., a small value of b) will choose to fire often. Similarly, large energy costs for spiking would imply lower firing rates. In fact, Fig. 8B shows that the overall firing rate of a cell is inversely related to its energy slope b, consistent with the principle of energy efficiency.

The good quantitative agreement between an optimally energy efficient code and the actual retinal code requires that both the energy costs and noise of neural symbols be taken into account. To demonstrate this point, we compared our model to two others: one which neglects the noise of transmission through a channel, and another which includes the empirical noise, but assumes all neural symbols have the same energy cost. As shown in Fig. 9A, models neglecting the cost of transmission (dashed line) fail to capture the rarity of large bursts, while models neglecting noise (dotted line) miss the suppression of noisy small bursts. By contrast, the full model (solid line) captures both the suppression of large, expensive bursts and small noisy ones as seen in the data (dots with error bars). Fig. 9B compares χ^2 of the fits to the data using the full and partial models. The dark and open circles represent models that neglect noise and energy costs, respectively. It is clear that a model incorporating both factors is a significant quantitative improvement.

DISCUSSION

In summary, we have argued that one aspect of the neural code of retinal ganglion cells, the distribution of burst sizes used to represent a broad stimulus ensemble, is surprisingly sensitive to both the noise and the energy cost of bursts. Retinal ganglion cells suppress the bursts with greater noise and greater metabolic cost, in both cases consistently with the principle of maximizing visual information per unit metabolic cost. The retina even appears to map stimuli preferentially onto less noisy firing events (see Fig. 3C). By measuring the noise in each firing event and estimating the energy cost up to one free parameter, we compared the actual burst size distributions of ganglion cells to the distribution that optimizes visual information per unit energy. Excellent agreement was found. These results suggest that the retina strives to use an energy efficient neural code.

Why should retinal energy efficiency matter to an animal, considering that the retina comprises only a small fraction of most vertebrates' bodies? In fact, neurons are some of the most energy-intensive cells in the body. For instance, the human brain accounts for 20% of daily energy intake but only 2% of body mass [Rolf and Brown, 1997]. Electrical and chemical signaling has been estimated to account for up to 85% of a neuron's energy budget [Atwell and Laughlin, 2001]. These data suggest that retinal neurons should attempt to conserve energy. Furthermore, the energy saved in the retina by an optimal code may underestimate the total savings for the animal. Retinal spike trains lead to cascades of synaptic currents and action potentials in the central brain, the costs of which might be reduced by using an efficient retinal code. Also, the retina employs much of the same molecular machinery – from ion channels to biochemical signaling cascades – found throughout the brain. As a result, mutations in this machinery that allow for greater energy efficiency in the retina may simultaneously enable other parts of the brain to save energy.

Despite these reasons, one might wonder why the efficient codes studied in this paper are important: photoreceptors are known to be metabolically expensive, and optimal coding does not affect this initial stage of the visual pathway. Ames [Ames, 1992] has made a detailed analysis of energy costs in the rabbit retina. He finds that while the photoreceptors do cost more ATP to run, the ganglion cell layer uses anaerobic respiration, so that its cost in terms of glucose consumption is comparable to the photoreceptor layer. Since the ganglion cell layer does not receive a direct blood supply in either the rabbit or salamander retinas, it is likely that the ganglion cell layer of salamander uses anaerobic respiration, too. In addition, a simple estimate of the total membrane area of the optic nerve in the salamander indicates that its energy cost may exceed the entire retina for reasonable firing rates, and this cost will be reduced by an efficient code.

The ability of neurons to use a metabolically efficient code must be selected for by evolution. We imagine that mutations which allow the retina to use an energy efficient code would leave the animal with identical visual behavior, but at a reduced metabolic cost. Determining the magnitude of the fitness advantage that arises from such a reduction in metabolic cost is very difficult. But even a slight fitness advantage can come to dominate a population: if the fractional fitness advantage is s, then the time necessary to spread through the population is 1/s generations [Gillespie, 1998]. Thus, a fitness advantage of one part in a million requires only a few million years to become widespread, which is fairly quick in evolutionary time. Evidence that eyes can be a significant expense to maintain is found from species of cave fish and salamanders that have adapted to environments without light ([Nelson, 1994]; [Roth, 1987]). In these species, the eyes have been fully or partially lost. Some, like Astyanax fasciatus mexicanus, have very close relatives that live outside caves and retain their eyes.

Our estimate of the energy cost of a burst left one free parameter, the energy slope b, measuring the relative cost of spiking to silence. This parameter took on a wide range of values when the model was fit to our data (see Fig. 8). What is a reasonable value of b? Our ion channel simulations suggest that the ion flow during a spike is ~ 100 times the leak current during 50 ms. However, the ganglion cell will have baseline metabolic costs in addition to the leak current. If we assume, following Siesjo and Ames, that half of the energy cost for ganglion cells is needed for baseline metabolism ([Siesjo, 1978]; [Ames, 2000]), and the other half for firing spikes at the observed rates of about 5 spikes/sec, then we estimate $b \sim 4$. However, we expect large variation from cell to cell due to differences in dendritic morphology, axon diameter, and ion channel densities [Roth, 1987]. The large range of observed firing rates (see Fig. 8A) suggests significant heterogeneity in our population of ganglion cells. In addition, one might interpret the energy cost parameter as including expenses of other neurons, like presynaptic bipolar cells or postsynaptic tectal cells, or as effectively including other constraints. It is worth considering whether these costs are relevant to the retinal code, and how they should be folded into our analysis. Clearly, more experimental data on the energy cost of neural signaling is needed.

Our analysis would benefit from several extensions. The first is developing a model that explicitly represents time. Because our model treats the spike train merely as an ordered list of firing events, it leaves out all of the information contained in the exact time at which each event occurs. In addition, we were forced to use an arbitrary time bin, 50 ms, to identify periods of silence as a zero-spike burst, which prevented us from predicting the overall firing rate of a ganglion cell. Other important extensions include testing energy efficiency for different functional types of ganglion cells, different species, and different stimulus conditions, to assess the generality of our result. It is of particular interest to see whether a given ganglion cell can maintain an energy efficient code when the statistics of its visual input change significantly.

This article raises interesting questions. We have shown that retinal ganglion cells use a code that suppresses noisy neural symbols. As the statistics of the visual input (such as light level or contrast) change, the noise also changes. In order to remain efficient, a ganglion cell would have to detect changes in its own noise and

adjust its code accordingly. How could this happen? The only likely method is for a cell to compare its responses to neighbors that are performing a similar function. This would suggest that a certain amount of redundancy is essential in ganglion cell function in order to enable adaptation to noise. If the picture of neurons as precise and robust information-bearing channels is correct, we must understand the mechanisms by which neurons detect and adapt to their own errors. Similarly, in the context of this paper, it is interesting to identify neural mechanisms for adapting to changing metabolic conditions.

Acknowledgments

We have enjoyed discussions with Larry Abbott, Bill Bialek, Kwabena Boahen, E.J. Chichlinsky, Mike deWeese, Gonzalo Garcia de Polavieja, Christof Koch, Simon Laughlin, Elad Schneidman, Peter Sterling, Chuck Stevens, and Gerard Toulouse. We are grateful to Don Kimber and Markus Meister for collaboration on previous work directly related to this article. During this project V.B. was supported initially by the Society of Fellows and the Milton Fund of Harvard University and later by DOE grant DOE-FG02-95ER40893. M.B. was supported by the Pew Charitable Trust and the E. Mathilda Ziegler Foundation. V.B. is grateful to the ITP, Santa Barbara and the Aspen Center for Physics for hospitality while this work was in progress.

References

- [Ames, 1992] A. Ames, 3rd. Energy requirements of CNS cells as related to their function and to their vulnerability to ischemia: a commentary based on retina. Can. J. Physiol. Pharmacol. 70:S158–S164, 1992.
- [Ames, 2000] A. Ames, 3rd. CNS energy metabolism as related to function. Brain Res. Rev. 34:42–68, 2000.
- [Arimoto, 1972] S. Arimoto. An algorithm for computing the capacity of an arbitrary discrete memoryless channel. IEEE Trans. on Info. Theory, IT-18:14–20, 1972.
- [Atick, 1992] J.J. Atick. Could information theory provide an ecological theory of sensory processing? Network 3:213–251, 1992.
- [Atwell and Laughlin, 2001] D. Atwell and S.B. Laughlin. An energy budget for signalling the grey matter of the brain. Submitted for publication.
- [Balasubramanian et.al., 2001] V. Balasubramanian, D. Kimber and M.J. Berry. Metabolically efficient information processing. Neural Computation, 13(4):799–816, 2001.

- [Barlow, 1961] H.B. Barlow. Possible principles underlying the transformation of sensory messages. In *Sensory Communication*, W.A. Rosenblith, ed. (MIT Press, Cambridge, MA), pp. 217-234 (1961).
- [Berry et.al., 1997] M.J. Berry II, D.W. Warland, and M. Meister. The structure and precision of retinal spike trains. Proc. Natl. Acad. Sci. USA, 94:5411–5416, 1997.
- [Berry and Meister, 1998] M.J. Berry II and M. Meister. Refractoriness and neural precision. J. Neurosci., 18:2200–2211, 1998.
- [Blahut, 1972] R.E. Blahut. Computation of channel capacity and rate distortion functions. IEEE Trans. on Info. Theory, IT-18:460–473, 1972.
- [Blahut, 1987] R.E. Blahut. *Principles and Practice of Information Theory*. Addison-Wesley, Massachusetts, 1987.
- [Buracas et.al., 1998] G.T. Buracas, A.M. Zador, M.R. deWeese, and T.D. Albright. Efficient discrimination of temporal patterns by motion-sensitive neurons in the primate visual cortex. *Neuron*, 20(5):959-969, 1998.
- [de Polavieja, 2001] G.G. de Polavieja Embid. Errors drive biological signaling to costly codes. Submitted for publication.
- [de Ruyter et.al.,1997] R.R. de Ruyter van Steveninck, G.D. Lewen, S.P. Strong, R. Koberle, and W. Bialek. Reproducibility and variability in neural spike trains. Science 275:1805–1808, 1997.
- [Fanselow and Nicolelis, 1999] E.E. Fanselow and M.A.L. Nicolelis. Behavioral modulation of tactile responses in the rat somatosensory system. J. Neurosci. 19:7603–7616, 1999.
- [Fohlmeister and Miller, 1997] J.F. Fohlmeister and R.F. Miller. Impulse encoding mechanisms of ganglion cells in the tiger salamander retina. J. Neurophysiol. 78:1935–1947, 1997.
- [Gillespie, 1998] J.H. Gillespie. *Population Genetics: A Concise Guide*. The Johns Hopkins University Press, 1998.
- [Laughlin et.al., 1998] S.B. Laughlin, R. de Ruyter van Steveninck, and J.C. Anderson. The metabolic cost of neural information. Nature Neuroscience 1(1):36–41, 1998.
- [Levy and Baxter, 1996] W.B. Levy and R.A. Baxter. Energy-efficient neural codes. Neural Computation 8:531–543, 1996.

- [McIlwain and Bachelard, 1985] H. McIlwain and H.S. Bachelard. *Biochemistry and the Central Nervous System, Fifth Edition*. Churchill Livingstone, London, 1985.
- [Meister et al., 1994] M. Meister, J. Pine, and D.A. Baylor. Multi-neuronal signals from the retina: acquisition and analysis. J. Neurosci. Methods 51:95–106, 1994.
- [Meister and Berry, 1999] M. Meister and M.J. Berry II. The neural code of the retina. Neuron (review) 22:435–450, 1999.
- [Nelson, 1994] J.S. Nelson. Fishes of the world, 3rd edition. John Wiley and Sons, New York, NY, 1994.
- [Rolf and Brown, 1997] D.F.S. Rolf and G.C. Brown. Cellular energy utilization and molecular origin of standard metabolic rate in mammals. Physiol. Rev. 77:731– 758, 1997.
- [Roth, 1987] G. Roth. Visual Behavior in Salamanders. Springer-Verlag, Berlin, 1987.
- [Schoenbaum, et.al., 1999] G. Schoenbaum, A.A. Chiba, and M. Gallagher. Neural encoding in orbitofrontal cortex and basolateral amygdala during olfactory discrimination learning. J. Neurosci. 19:1876–1884, 1999.
- [Siesjo, 1978] B. Siesjo. Brain Energy Metabolism. Wiley, New York, 1978.
- [Smirnakis et al., 1997] S.M. Smirnakis, M.J. Berry, D.K. Warland, W. Bialek, and M. Meister. Adaptation of retinal processing to image contrast and spatial scale. Nature 386:79–83, 1997.
- [Strong et.al., 1997] S.P. Strong, R. Koberle, R.R. de Ruyter can Steveninck, W. Bialek. Entropy and information in neural spike trains. Phys. Rev. Lett. 80:197–200, 1997.
- [van der Schaaf and van Hateren, 1996] A.A. van der Schaaf and J.H. van Hateren. Modelling the power spectra of natural images statistics and information. Vision Res. 36:2759–2770, 1996.
- [van Hateren, 1992] J.H. van Hateren. Real and optimal neural images in early vision. Nature 360:68–70, 1992.
- [Wong-Riley, 1989] M.T.T. Wong-Riley. Cytochrome oxidase: an endogenous metabolic marker for neuronal activity. Trends Neurosci. 12:94–101, 1989.

CAPTIONS

Figure 1: Burst size distributions for four representative salamander ganglion cells, showing (A) very exponential shape, (B) significant suppression of small bursts, (C) and (D) flattening of the distribution for small bursts.

Figure 2: (A) Simplified schematic of our model of a sensory system. (B) and (C) Effects of noise in the model: the optimal usage probabilty of each symbol is plotted for different levels of noise. In both (B) and (C), there are 6 output symbols, and the energy cost of symbol k is $E_k = k$. In (B), the noise matrix has the following "diagonal" form: $\Pr(z|y) = 0$, except for $\Pr(z = k|y = k) = 1 - 2p$ for $k = 1 \cdots 6$; $\Pr(z = k + 1|y = k) = \Pr(z = k - 1|y = k) = p$ for $k = 2 \cdots 5$; $\Pr(z = 2|y = 1) = \Pr(z = 5|y = 6) = 2p$. The optimal usage distribution is exponential when p = 0, showing suppression of energetically expensive symbols. As the noise increases, there is a marked deviation from an exponential symbol distribution. In (C), the noise matrix is of the same form as in (B), but with p = 0.1 for all k except k = 3, for which the noise probabilities are varied. This panel shows that noise in a single symbol strongly supresses the use of that symbol in the optimal distribution.

Figure 3: (A) Variance of the spike count in a firing event plotted as a function of average spike number for 1043 events. (B) Deterministic mapping of stimulus to presymbol: noisy boundary versus reliable core. Visual stimuli occupy a large space, where each point is a pattern of light intensity as a function of time (shown on far left). This stimulus space $\{X\}$ is mapped deterministically into presymbols $\{Y\}$, which are in turn mapped into the output symbols $\{Z\}$ by the noise matrix. The figure shows two regions of presymbol space which should be mapped into one or two spikes, respectively, in the absence of noise. In the presence of noise, stimuli that are mapped into the core of these regions will be reliably encoded into the same number of spikes, while stimuli mapped into the boundary regions as marked will be readily corrupted, being transmitted sometimes as one spike and sometimes as two. See the text for discussion. (C) Histogram of different presymbols used by one ganglion cell.

Figure 4: (A)–(C) Distribution of spike counts for three representative firing events of types 2, 1/2, and 0/2. (D) Depiction of the noise matrix for a ganglion cell with the transition probability $Q_{z|y}$ for a presymbol y to emerge as an output symbol z plotted in greyscale.

Figure 5: Ion channel simulations: (A) Regular spiking behavior seen in the voltage response V of the Fohlmeister-Miller model (top panel) to current pulses $I_{\rm ext}$ of varying durations (bottom panel). (B) Associated currents through the cell membrane, including voltage-gated sodium $I_{\rm Na}$, delayed rectifier potassium $I_{\rm K}$, potassium A-current $I_{\rm A}$, voltage-gated calcium $I_{\rm Ca}$, calcium-gated potassium $I_{\rm K(Ca)}$, and leak $I_{\rm leak}$.

Figure 6: Total charge flow in the Fohlmeister-Miller model plotted as a function of the number of spikes in a 50 ms period. For the delayed rectifier potassium current, a linear curve fit is shown as a dashed line.

Figure 7: Curve fits of an optimally energy efficient code to the experimental burst size distribution for four cells made by finding the best value of the energy cost parameter b. Dots with error bars are the experimental data; the heavy central line is the fit. The thin upper and lower lines are numerically estimated upper and lower ranges on the theoretical fit arising from propagation of the error bars in the noise matrix through the theory (see Materials and Methods). Values of (χ^2, b) for cells in (A)–(D) are (1.6, 1.1), (5.1, 0.6), (7.2, 1.0), and (1.6, 2.6), respectively.

Figure 8: (A) Goodness-of-fit (χ^2) plotted versus best energy slope (b) for each ganglion cell. Range bars are obtained from numerical propagation of uncertainty in the noise matrix (see text for discussion). (B) Overall firing rate plotted versus energy slope for each ganglion cell.

Figure 9: (A) Experimental burst size distribution (circles) for a ganglion cell shown against the full optimal model (dark line) as well as models without noise (dotted line) and without energy (dashed line). The full model is seen to match the data significantly better than either partial model. (B) The χ^2 deviation between the burst size distribution of model and data for partial models without noise (dark circles) and without energy (open circles) plotted against χ^2 for the full model. The dashed line shows the case where the partial and full models have the same error.

Figure 1

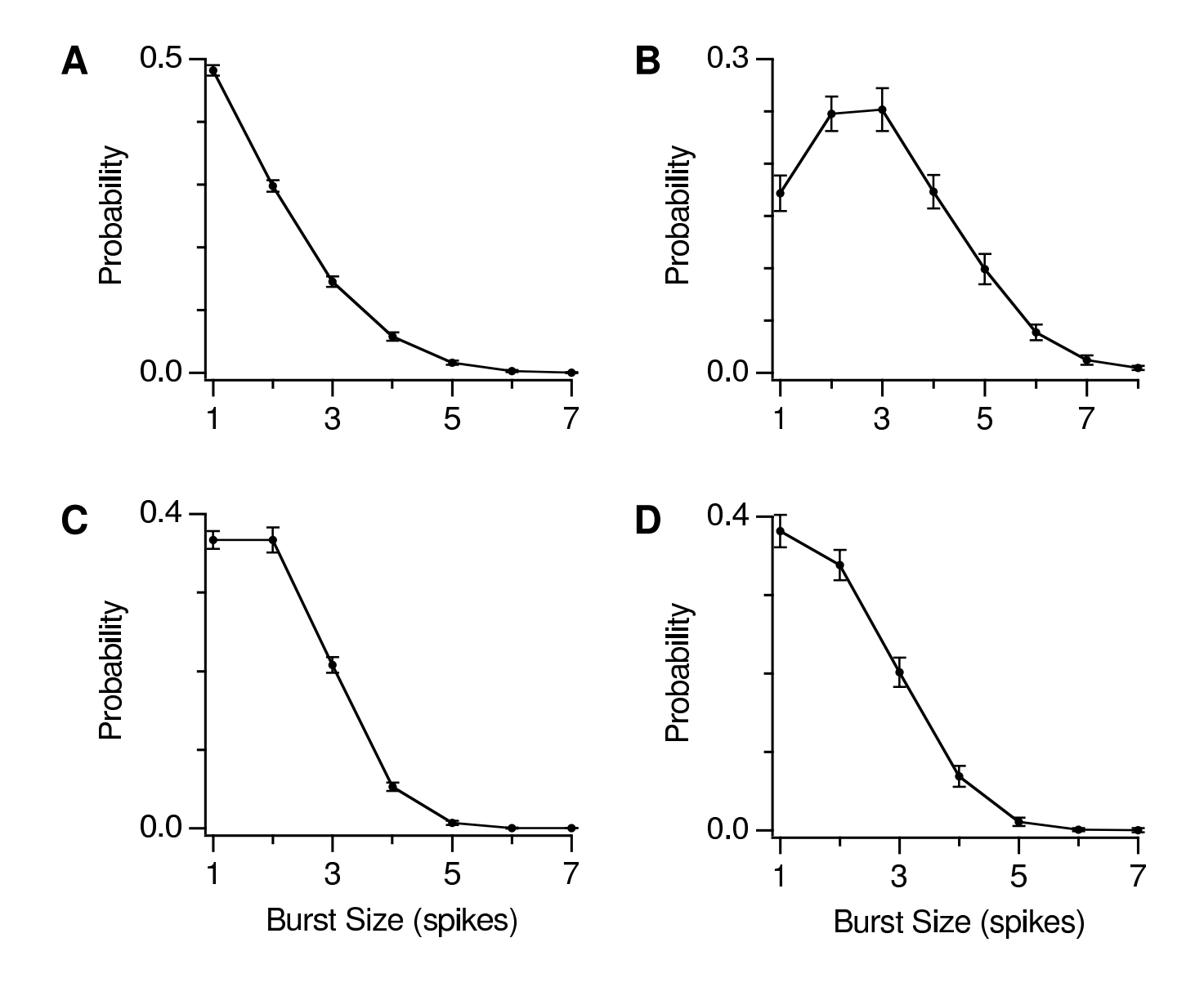


Figure 2

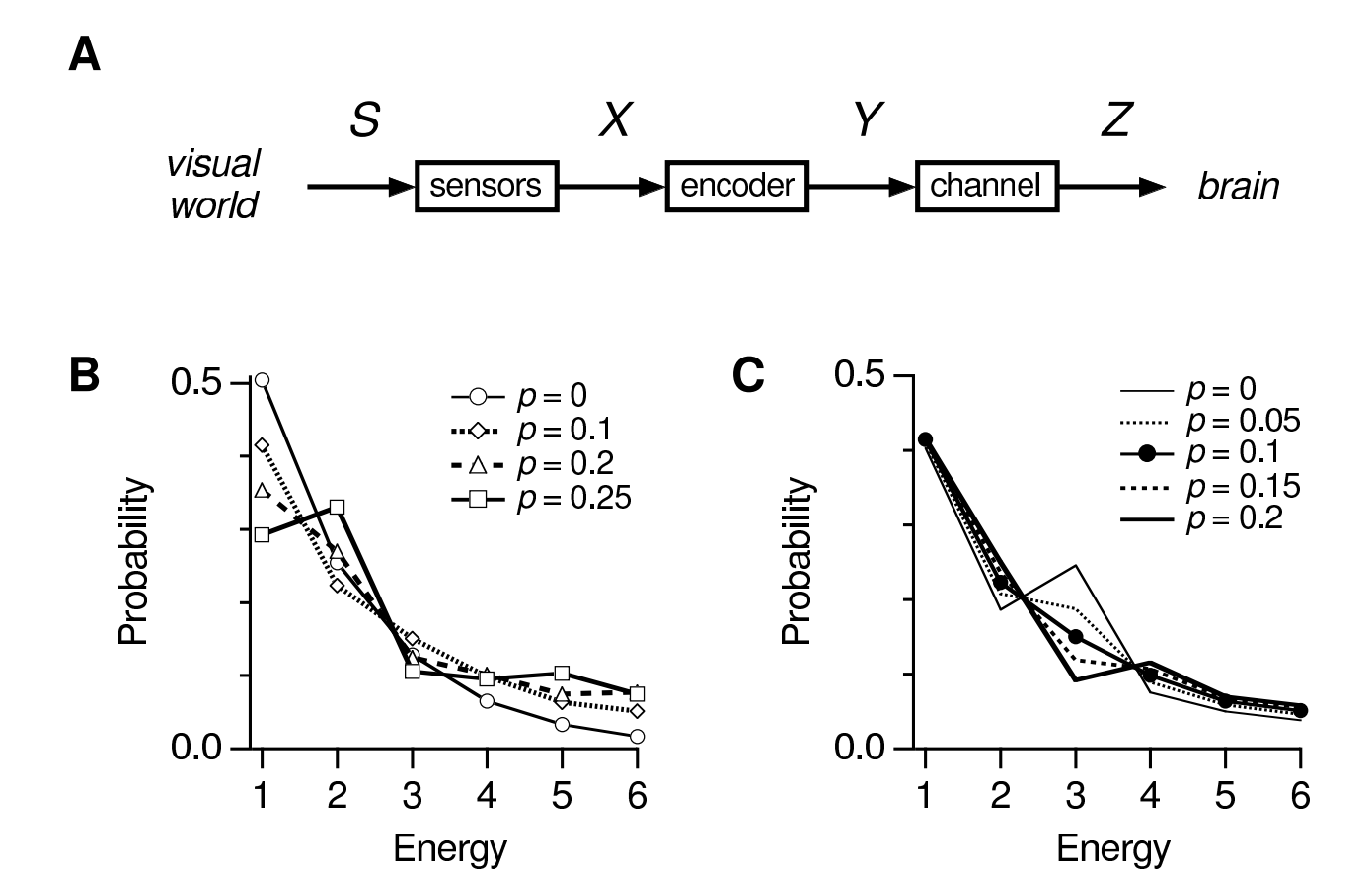
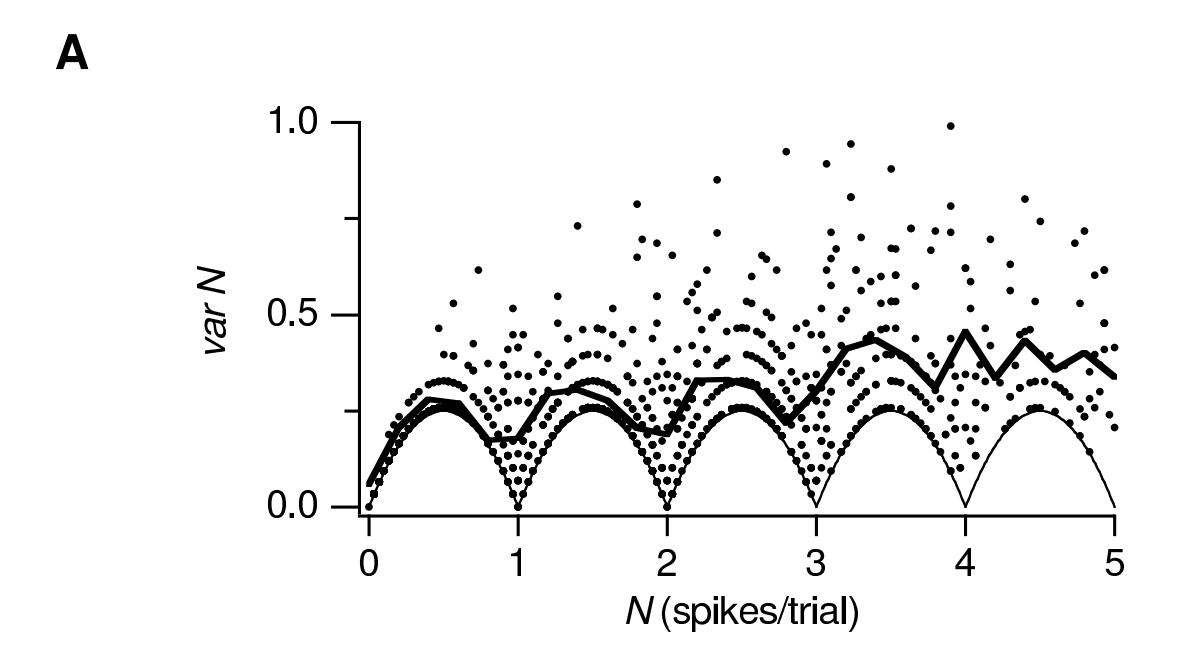
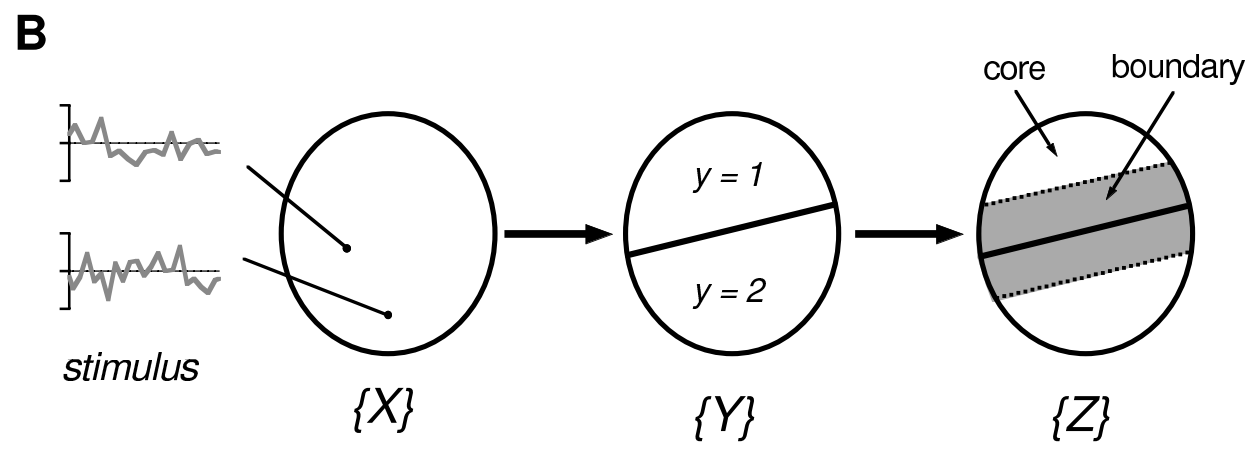


Figure 3





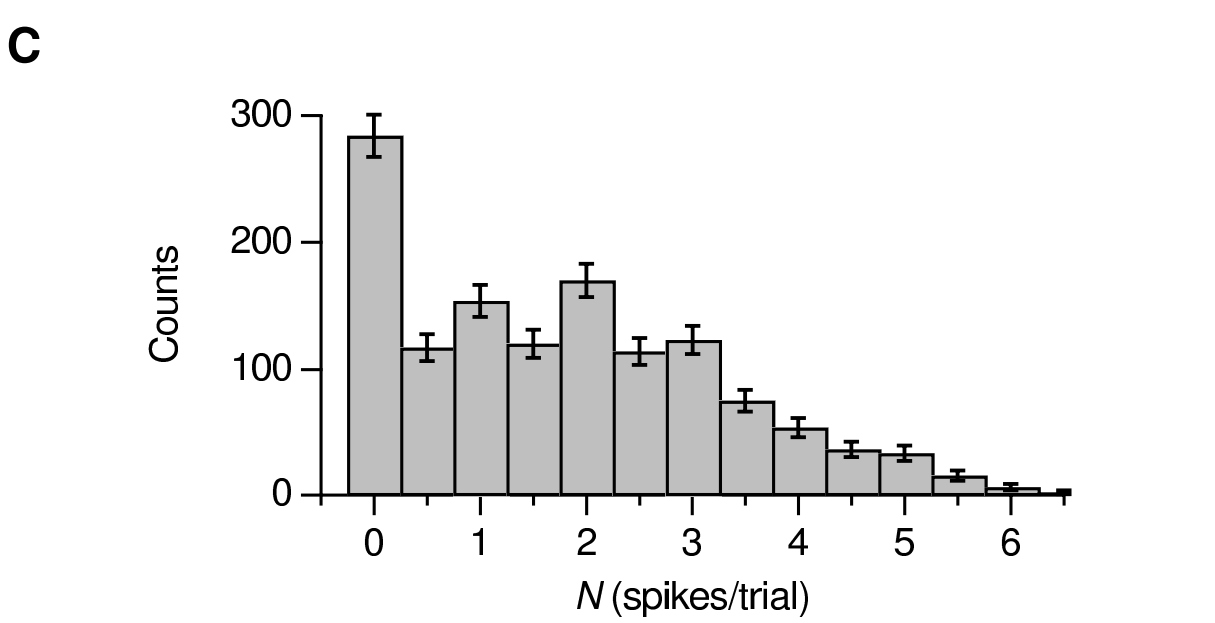


Figure 4

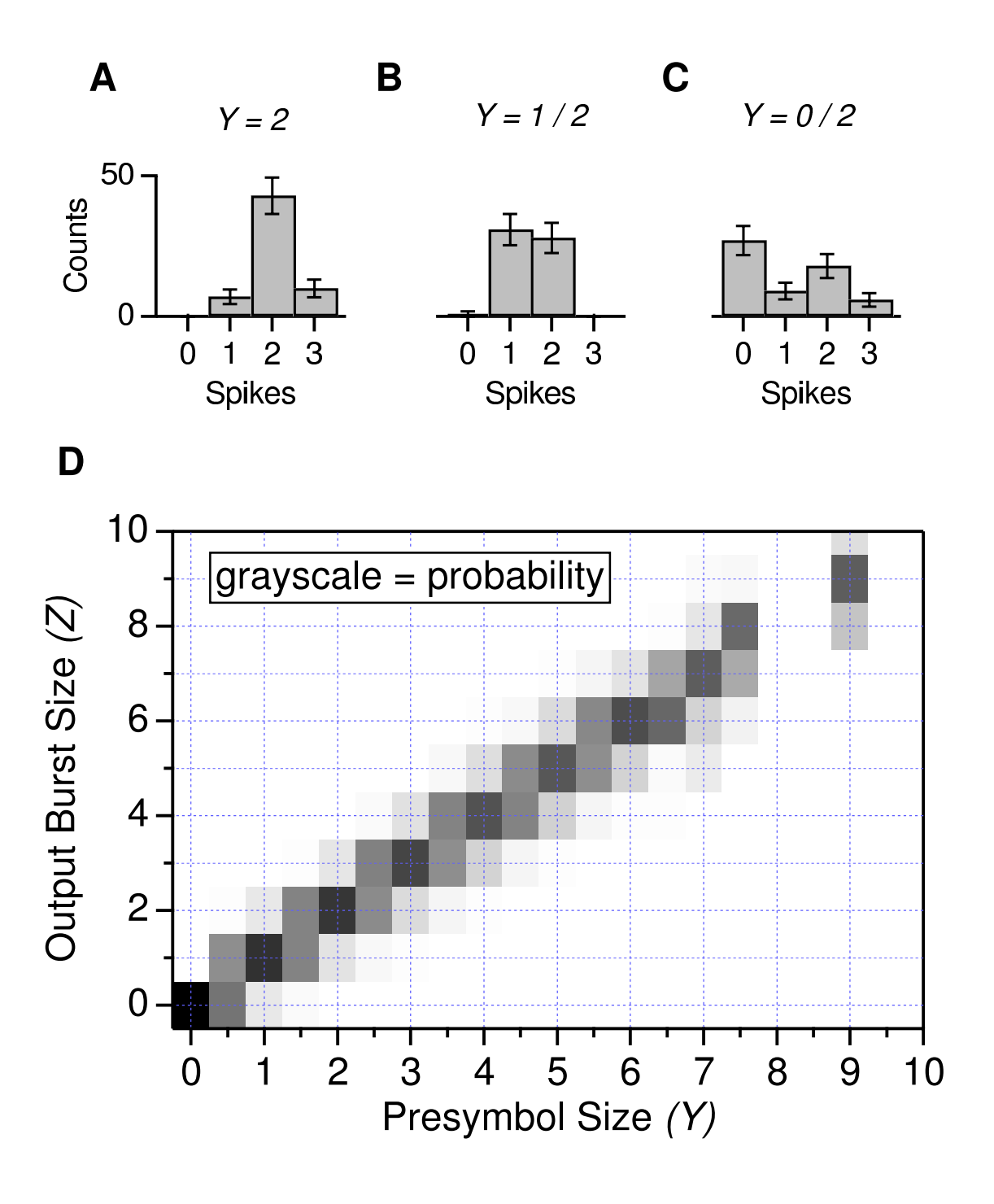
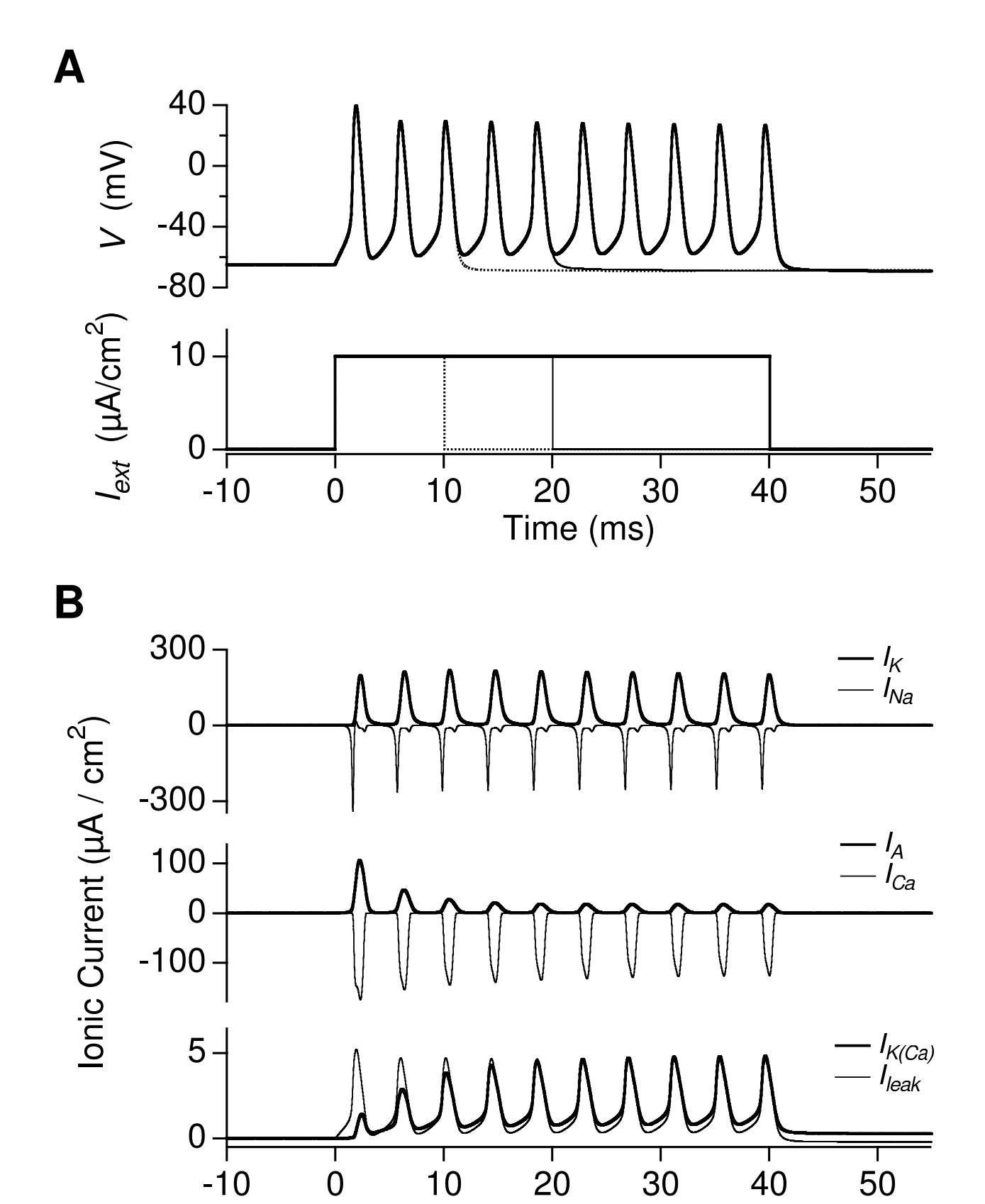


Figure 5



Time (ms)

Figure 6

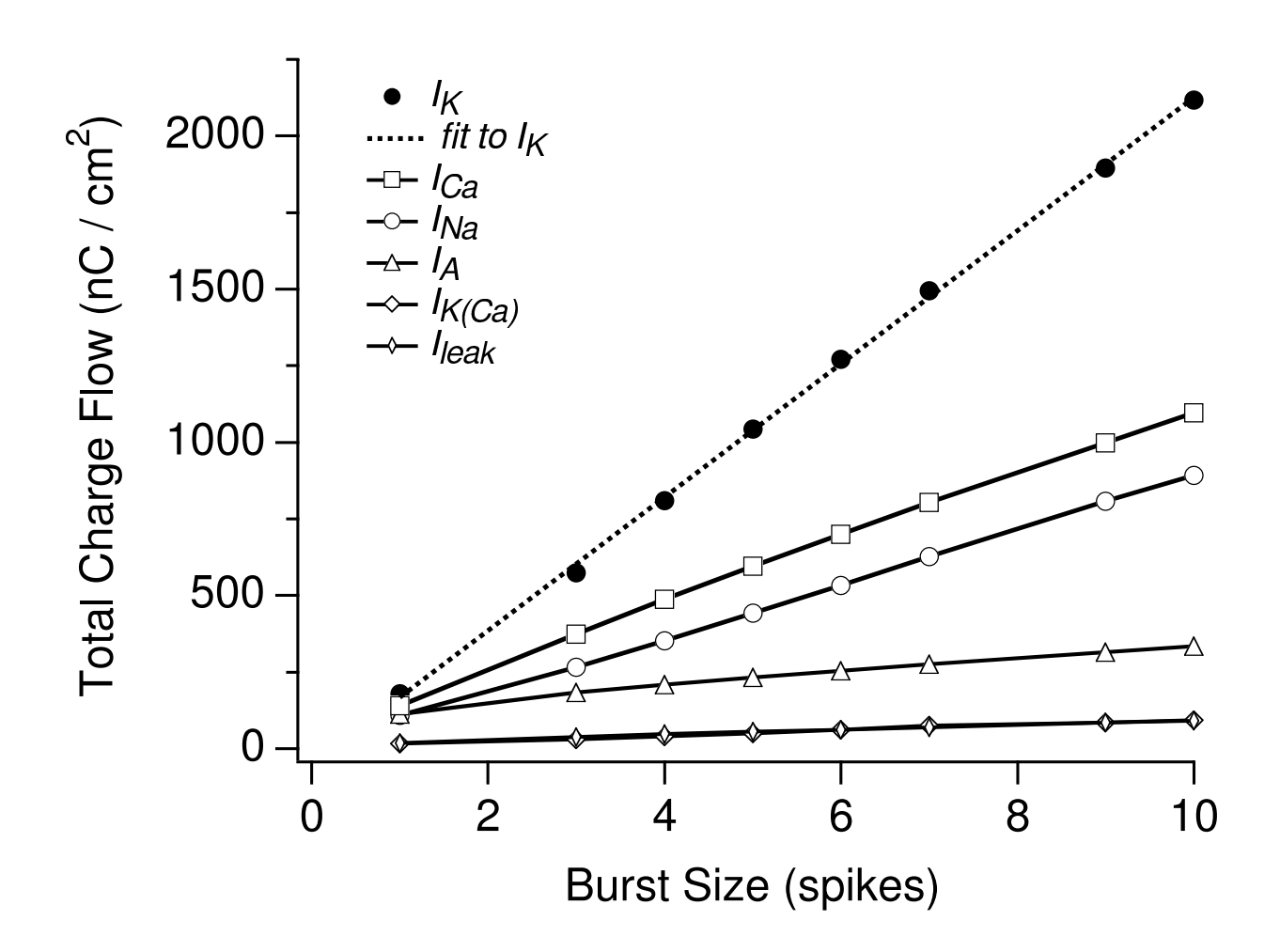


Figure 7

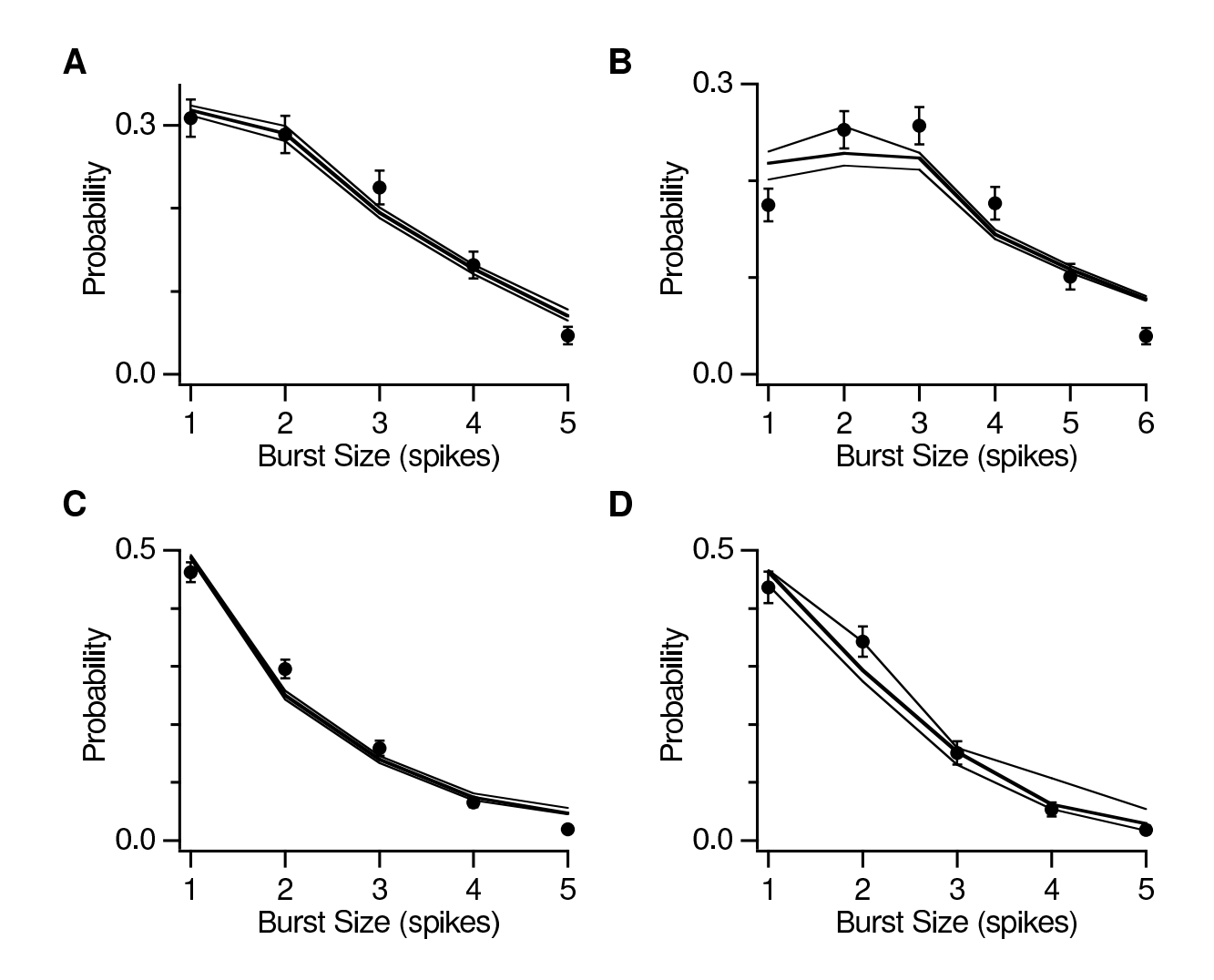
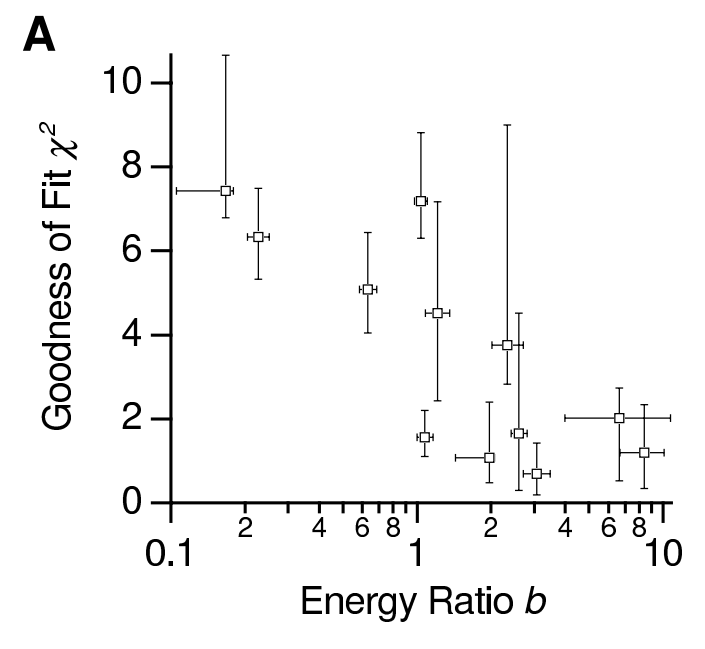


Figure 8



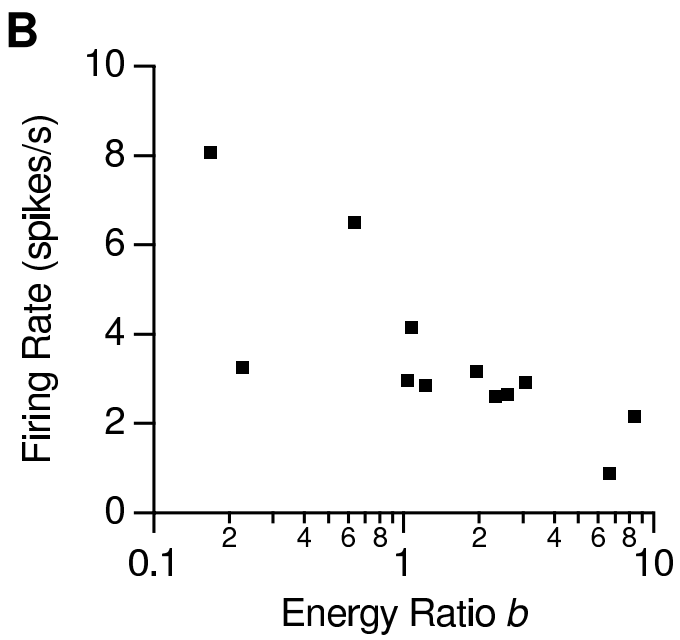


Figure 9

